*Chapter*

# ORGANOMETALLIC-METALLIC-CYCLOTRIPHOSPHAZENE MIXTURES: SOLID STATE METHOD FOR METALLIC NANOPARTICLE GROWTH

***C. Diaz[1,*], M. L. Valenzuela[2] and C. O'Dwyer[3,4]***

[1]Departamento de Química, Facultad de Ciencias, Universidad de Chile, Santiago, Chile

[2]Universidad Andrés Bello, Departamento de Ciencias Química, Facultad de Ciencias Exactas, Santiago, Chile

[3]Department of Physics and Energy, University of Limerick, Limerick, Ireland

[4]Materials and Surface Science Institute, University of Limerick, Limerick, Ireland

## ABSTRACT

We review a recent general solid state method to obtain metallic, metal oxide and phosphate nanoparticles and crystals by pyrolysis at 800 °C using organometallic derivatives of cyclo and polyphosphazene precursors containing diverse organometallic fragments linked to polymeric or oligomeric phosphazenes. When the preparation of the molecular precursor is not possible or results in low yield, an alternative

[*] Corresponding author's email address: cdiaz@uchile.cl.

method using solid state mixtures of the type $MLn/N_3P_3[O_2C_{12}H_8]_n$, where MLn can be a single metallic salt, and a coordination compound or an organometallic, is possible. For $AuCl(PPh_3)/[NP(O_2C_{12}H_8)]_n$ mixtures, single crystal cubic Au nanoparticles form, whose morphology, crystal shape, size and distribution strongly depends on deposition quantity and the mixture molar ratio. Nanoparticles as small as 3.5 nm are observed if the mixture is prepared in a crucible and varied geometries of microcrystals found when the mixture was deposited on Si or $SiO_2$ wafers, including single-crystal gold fullerene structures. Extension to Ag, Pd and Re-containing precursor mixtures such as $Ag(PPh_3)(CF_3SO_3)/ [NP(O_2C_{12}H_8)]_3$, $PdCl_2/N_3P_3[O_2C_{12}H_8]_3$, and $KReO_4/N_3P_3[O_2C_{12}H_8]_3$ allows microcrystal formation during pyrolysis. A thermally induced phase demixing mechanism describes the evolution of the crystal growth, aided microphase separation of the polymer mixture. This microphase demixing is shown to be an overarching mechanism involved in the nano to micro scale growth of crystals. A probable mechanism of the atomic and molecular-level chemistry is also proposed based on decomposition of the macromolecular polymeric, trimer and oligomeric precursors for the initial stages.

## INTRODUCTION

Nanoparticles have attracted extensive research interest, mainly due to their size-dependent properties and great potential for many applications [1-3]. There are two main ways for the preparation of nanomaterials: those in solution and those in solid state. The greatest development has been in solution, while solid state approaches are scarce. The main solid state methods to prepare and synthesize nanoparticles have been recently discussed, [4, 5] and in stark contrast with the hundreds of solution-based reports, as little as four routes to grow Au nanoparticles completely in the solid state are known at the time of writing. A similar situation holds for Ag nanoparticles where only two solid-sate methods have been reported. The aim of developing solid state methods to prepare nanoparticles stems mainly from their possible application in solid state materials and powder-oriented applications, from thin film metal deposition to noble metal nanoparticle-carbon catalysts, oxide growth, photonic and dielectric materials, to new materials for Li-ion rechargeable batteries.

The ability to rationally prepare metallic and metal oxide nanoparticles stems from the exploring methods for alternative nanoscale metal deposition in solid state nanoelectronics and nanotechnology [6-8] and the benefit of being

able to deposit both metals and dielectric or semiconducting oxides, both from the same base route.

Issues including limitations on good mechanical and thermal stability of nanoscale metals have been found to be related to certain deposition methods for these metals [8]. A new solid state method to obtain metallic nanostructured have reported recently for materials of the type: M, $M_xO_y$ and $M_xP_yO_z$ for a range of transition, valve and noble metals, using organometallic derivatives of poly and cyclotriphosphazenes as molecular precursors, summarized in Figure 1. [9-26]

Briefly, the method consists of the pyrolysis of the molecular or macromolecular precursors at 800 ºC under air. The resulting product depends strongly on the nature of the metal. Thus for metals such as Cr [9, 10], Ru [17] and Mo [21] where the metal oxide is easily formed, the respective nanostructured metal oxides are observed. On the other hand, in other cases such as with Mn [11], Sn [22, 23] and Fe [24], only the respective nanostructured pyrophosphate was observed. With metals and metalloids such as Ti [15], Si [18, 22, 23] and W [12], both phases were observed, *i.e.* the metal oxide and the pyrophosphate. With noble metals for which the formation of oxides or pyrophosphates is thermodynamically unfavored, the reduction with CO produced during molecular decomposition in the pyrolysis process, allowed the formation of nanostructured M° [19, 20, 25].

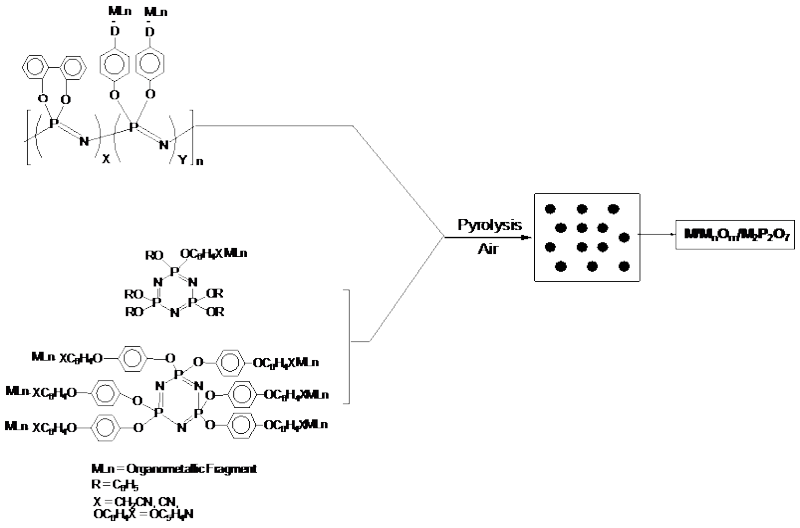


Figure 1. Schematic representation of the solid state method for nanostructured material formation using oligomeric and polymeric precursors.

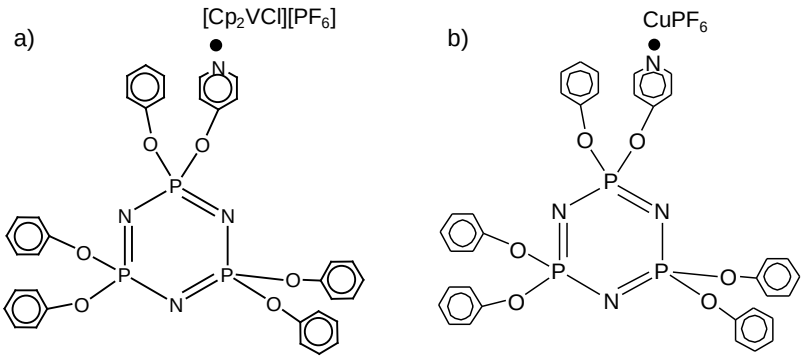


Figure 2. Representative formulas of $[N_3P_3(OC_6H_5)_5OC_5H_4N{\bullet}Cp_2VCl][PF_6]$ and $N_3P_3[OC_6H_5]_5[OC_5H_4N{\bullet}Cu][PF_6]$.

While the process has now been well established for a range of metals, giving a smorgasbord of oxide and phosphate based nanostructured materials all by a similar route, some metals can be difficult to prepare in such form and some are often unsuccessful. Good examples are the sensitively multivalent vanadium and copper derivatives of cyclotriphosphazene, as shown in Figure 2, and only $[N_3P_3(OC_6H_5)_5OC_5H_4N{\bullet}Cp_2VCl][PF_6]$, $N_3P_3[OC_6H_5]_5[OC_5H_4N{\bullet}Cu][PF_6]$ and $N_3P_3[OC_6H_4CH_2CN{\bullet}CuCl]_6[PF_6]_6$ have been prepared, but in relatively poor yields compared to metals and metalloids described earlier.

Furthermore by using the polymer $[\{NP(O_2C_{12}H_8)\}_{0.7}\{NP(OC_5H_4N\text{-}4\{Au(C_6F_5)_2\}_{0.3}]_n$ as a precursor, a 3-D network of porous Au can be obtained instead the expected Au nanoparticles [20]. This and the previously mentioned V and Cu cases, could be solved using adequate $MLn/N_3P_3[O_2C_{12}H_8]_n$ mixtures. In fact, by pyrolyzing the $AuCl(PPh_3)/[NP(O_2C_{12}H_8)]_n$ mixtures, nanoparticles as small as 3.5 nm were obtained [26]. This chapter reviews the latest progress using these new methods with several important noble metals: Au, Ag, Pd and Re.

## THE SOLID STATE PRECURSOR MIXTURES (SSPM) METHOD

The method is highly sensitive to the preparation procedure. Two main procedures can be used: pyrolyzing the material in a crucible or pyrolyzing a deposited sample on Si or $SiO_2$ wafers, as summarized in Figure 3.

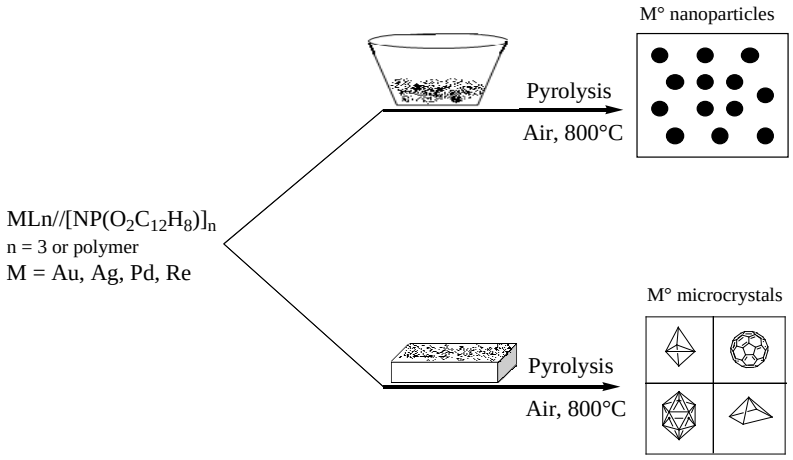


Figure 3. Schematic representation of the SSPM method.

As detailed elsewhere [9-26], specific differences in overall organometallic and cyclotriphospahzene chemistry allows a range of systems. The following describes details of this new approach for Au, Ag, Pd and Re.

## MIXTURES OF AUCL(PPH3) AND [NP(O2C12H8)]N

Some of these results have been recently reported [26] and here we briefly describe the method itself and summarise the unique observation of a variety of gold morphologies possible through a single solid state method. We used mixtures comprising $AuCl(PPh_3)/[NP(O_2C_{12}H_8)]_3$. The results indicate that both the morphology and the size particles of the products depend strongly on the preparation procedure. The mixtures are made in dichloromethane as solvent and separation of the solid product is performed using the following methods:

a) *Film*: A $CH_2Cl_2$ solution of the respective mixtures of $AuCl(PPh_3)$ and the trimer or polymer is allowed to evaporate slowly to cast a film that is dried at room temperature.
b) *Powder (I)*: The respective molar mixture of $AuCl(PPh_3)$ and the cyclotriphosphazene or polyphosphazene is dissolved in dichloromethane stirred for 24 hours and evaporated to dryness in a vacuum at 70 °C.

c) *Powder (II)*: The respective molar mixture of $AuCl(PPh_3)$ and the respective trimer or polymer is dissolved in THF, stirred for 24 hours and evaporated to dryness in a vacuum at room temperature.

The resultant solids from procedures a) to c) are then placed in a crucible and pyrolyzed at 800 °C under air. In all cases the products were identified to be Au by their XRD patterns, which show the (111), (200), (220), and (311) crystal reflections that can be indexed as fcc. The $I_{(220)}/I_{(111)}$ ratio was somewhat higher that observed for Au bulk (0.32) indicating an preferred (110) termination in resulting materials. A representative XRD pattern is shown in Figure 4a. The red bars are the patterns of standard cubic gold (JCPDS 004-0784).

Consistently, the diffraction electron patterns exhibit polycrystalline rings with diameters in ***k***-space corresponding to the (111), (200), (220) and (311) planes. While crystallographically, all products can be classified as single crystal or polycrystalline cubic Au, the principal difference in all Au products using this method are the resulting particle morphologies; variants including fused granular networks, low density metallic foams and nanoparticles can be formed. A summary of the main morphological variants and particle size (where relevant) are summarized in Table 1.

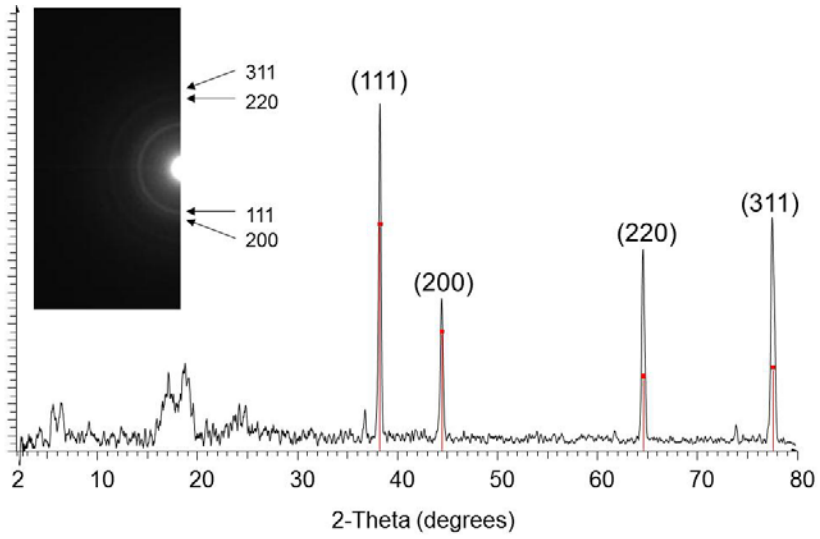


Figure 4. (a) X-ray diffraction pattern of the pyrolytic residue from 1:1 $AuCl(PPh_3)/[NP(O_2C_{12}H_8)]_3$ mixture. The inset shows the corresponding electron diffraction pattern.

**Table 1. Summary of the main properties of the as-prepared Au nanoparticles from precursor mixtures**

| Mixture[d] | Polymer/Au | Trimer/Au | Morphology | Particle size (nm)[e] |
|---|---|---|---|---|
| 1a | 1//1[a] | | | 3.5 |
| 2a | 3//1 [a] | | Dense grains | |
| 1b | 1//1[b] | | | 75 |
| 2b | 3//1 [b] | | Dense grains | |
| 1c | 1//1[c] | | Porous | |
| 2c | 3//1 [c] | | Foam | |
| 3c | 5//1 [c] | | Foam | |
| 1'c | | 1//1 [c] | Foam | 4.7 |
| 2'c | | 3//1 [c] | Fused grains | |
| 3'c | | 5//1 [c] | Fused grains | 6.5 |
| 4'c | | 10//1[c] | 3-D Porous network | |

[a] Film; [b] Powder (I); [c] Powder (II); [d] Mixture Polymer/Au (1,2,3…n) or Trimer/Au (1',2' 3'…n' etc.) prepared according to method a), b), or c).[e] Measured by TEM using a histogram analysis.

As summarized in Table 1, the smallest individual entities are nanoparticles obtained using a 1:1 phosphazene/AuCl ($PPh_3$) ratio using preparation methods a) to c). In several cases metal foams [27-33] are obtained.

Previous solid state methods for preparing Au nanoparticles involved heating by the Brust method, which gives nanoparticles with diameters in the range 3.4-9.7 nm [34-36] and in some cases, nanoparticles trapped in solid glass materials are possible by irradiating a solid mixture containing the silicate glasses and $Au_2O_3$ [37]. Using this approximation, gold nanoparticles in the range 6-8 nm was obtained. Also, glasses containing Au nanoparticles with composition $15CaO•5P_2O_5•80SiO_2$ have been reported [38]. Au nanoparticles and microparticles were obtained, tuned by the calcination temperature: 1.5-2.5 nm at 150 °C, ~30 nm at 600 °C and between 30-200 nm in diameter when formed at 900 °C. More recently [39], in a similar approximation the glass $80SiO_2•20Na_2O•10CaO$ was doped with $AuCl_3•2H_2O$ and irradiated using synchrotron radiation. After calcination at 1450 °C, the resulting Au nanoparticles ~3.2 nm in size were generated inside the glass material.

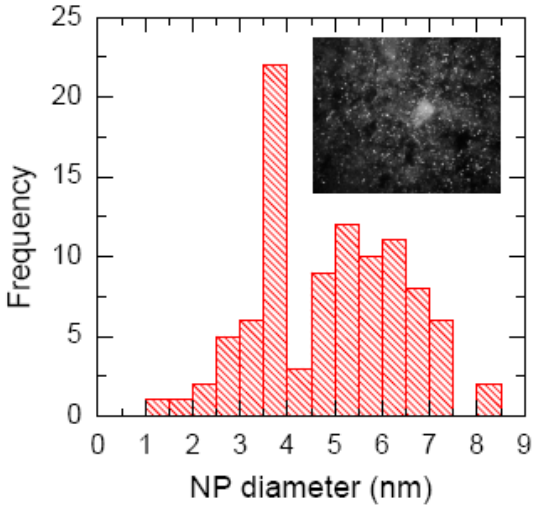


Figure 5. The diameter distribution profile confirms a bimodal Gaussian spread in diameters with 95% of NPs having diameters in the range 3.7-4.0 nm. *Inset*: Dark field TEM image of gold NPs formed in the demixing polymer mixture. In dark field, the brighter labyrinthine regions constitute the polymer and bright points are the Au NPs.

For Au, using this SSPM method, we have shown that the variation of the phosphazene/Au ratios allows for the formation of either metallic foams of high density or discrete Au NPs, whose mean size and morphology are controlled by the structure of the precursor constituents and the relative ratio in the mixtures. With the $[NP(O_2C_{12}H_8)]_n$/$AuCl(PPh_3)$ mixtures, Au NPs of 3.5 nm diameter were obtained from films formed through pyrolysis of the 1:1 mixture ratio, while with the analogous 1:1 mixture of $N_3P_3(O_2C_{12}H_8)_3$/ $AuCl(PPh_3)$ resulted in Au NPs with a mean diameter of 4.7 nm from a powder deposit.

An example of Au NP size distribution and physical location throughout the decomposed polymeric matrix using HAADF TEM is shown in Figure 5. Comparison with previous studies shows that the formation of metallic nanostructures does not require the covalent linking of the organometallic fragment to the polymeric or trimeric phosphazenes, although the presence of the cyclic or polymeric phosphazene as solid state template is necessary. The method allows the tuning of the resultant Au product; the Au is phase pure, single crystal and can be formed as small NPs or as low density, high surface area foams completely in the solid state. Interestingly, using the SSPM method, in some deposits where the density of Au is kept highest, the formation of gold metal foams was observed and attributed to spinodal

decomposition during demixing of the Au-containing phase and the polymer phase, resulting in a 3D spinodal network of polycrystalline high surface area gold. Metal foams are a relatively new class of materials with unique combinations of properties such as high stiffness, low density, gas permeability and thermal conductivity [27-33]. As such these materials promise to enable new technologies in areas as diverse as catalysis, fuel cells, hydrogen storage and thermal and acoustical insulation. Preparative methods for making metal foams to date have somewhat limited in scope, the most common typically that of de-alloying of the bimetallic $Au_{022}Ag_{0.58}$ [27,28]. The here presented method could be a new useful way to these type of materials. Figure 6 shows the various foam-like morphologies possible at high Au loading of the organometallic-polymer mixture. In each porous structures shown in Figure 6, the entire porous material is pure monocrystalline gold.

More interesting results were obtained pyrolyzing the Au mixtures on Si and $SiO_2$ wafers [20] and observing the products by SEM. The methods for anchoring pyrolyzed products have been reported previously [20].

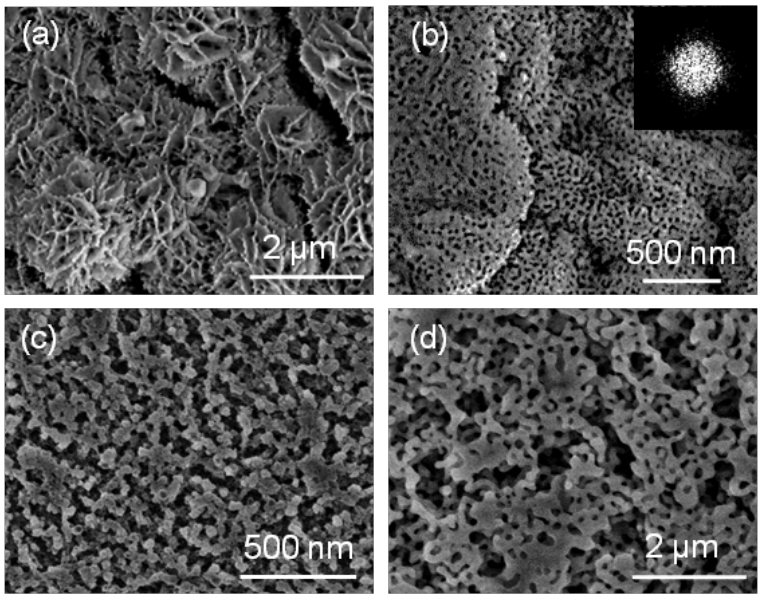


Figure 6. (a-d) Various density high surface area foam-like polycrystalline gold structures formed after pyrolysis of respective precursor mixtures with a high Au content. Inset: FFT of the porous gold showing a characteristic wavelength indicative of spinodal decomposition during the demixing of the two polymeric phases, one of which contains gold.

Briefly, a solution of the mixture was dropped on Si or $SiO_2$ wafers and pyrolyzed at 800 °C under air. SEM or AFM measurements were performed on the crystals formed on the wafers. When the phosphazene/AuCl($PPh_3$) mixtures were deposited on Si or $SiO_2$ wafers, Au microcrystals were observed. Previous attempts to obtain structured gold NPs by pyrolysis of polyphosphazenes containing AuCl covalently bonded to the polymer backbone by coordination to pendant -O-$C_6H_4$-$PPh_2$ substituents [25] were unfruitful; only diffuse and randomly shaped and sized Au particles were found.

We performed analogous pyrolytic experiments with physical mixtures of $AuCl(PPh)_3$ and the cyclic or polymeric phosphazenes $[N_3P_3(O_2C_{12}H_8)_3]$ or $[NP(O_2C_{12}H_8)_2]_n$ ($O_2C_{12}H_8$ = 2,2´-dioxy-1,1´-biphenyl) (Figure 7) that have $\lambda^5$-dioxydiaryl groups in the repeating units (poly-spirophosphazenes) [40]. The growth steps of the tetrahedral gold microcrystals from triangular platelets to full tetrahedra are shown in Figure 7(a,b), where we observe coarsening of Au NPs formed in the intial stages of decomposition, to the pinhole voids formed during nucleation dewetting of the polymer mixture. The gold comes from one phase, the other being polymeric and demixing occurs under thermal excitation. Compositional analysis using EDX and XPS confirms that the features within pionhold voids are pure gold and the resulting polyhedral crsytals that are formed (Figure 7) are also pure cubic gold. Higher resolution analysis of individual crystals (Figures 7b-d) shows the variety of crystal shapes possible through coarsening of NPs formed by cleavage of metal centers through a decomposing polymer without needing surfactants [41]. The remarkable observation is the subsequent growth of crystals (uniquely from these pinholes), subsequent Ostwald ripening of nanoparticles by migration of the NPs to each pinhole void formed during demixing, and the eventual growth of the crystals.

A variety of individual crystal shapes are found; icosahedra, tetrahedra (which also develop into octahedra), heptahedra, cuboctahedra, decahedra and truncated icosahedra (fullerene-shaped) crystals of similar size are all formed through simple pyrolysis.

The fullerene-like crystals shown in Figure 7d [42,44] are, to the best of our knowledge, the first to be observed for Au on any length scale. The tetrahedra evolve symmetrically, where the edge length is first defined by forming a platelet which evolves to three-fold rotational symmetry from asymmetric hexagonal platelets where the vertices are terminated by a {111} facet; subsequent growth upfills the structure until a geometrically perfect tetrahedron is formed.

The method relieves the constraint on solution based methods that use surfactants to control particle size and shape and the approach and can be directly applied to many other transition and noble metals capable of coordination to the organometallic derivative. This bottom-up single-step approach for molecular level metal-polymer building blocks provides the often sought solid state route to polyhedral metallic crystal growth without the need for ligands or surfactants to influence shape.

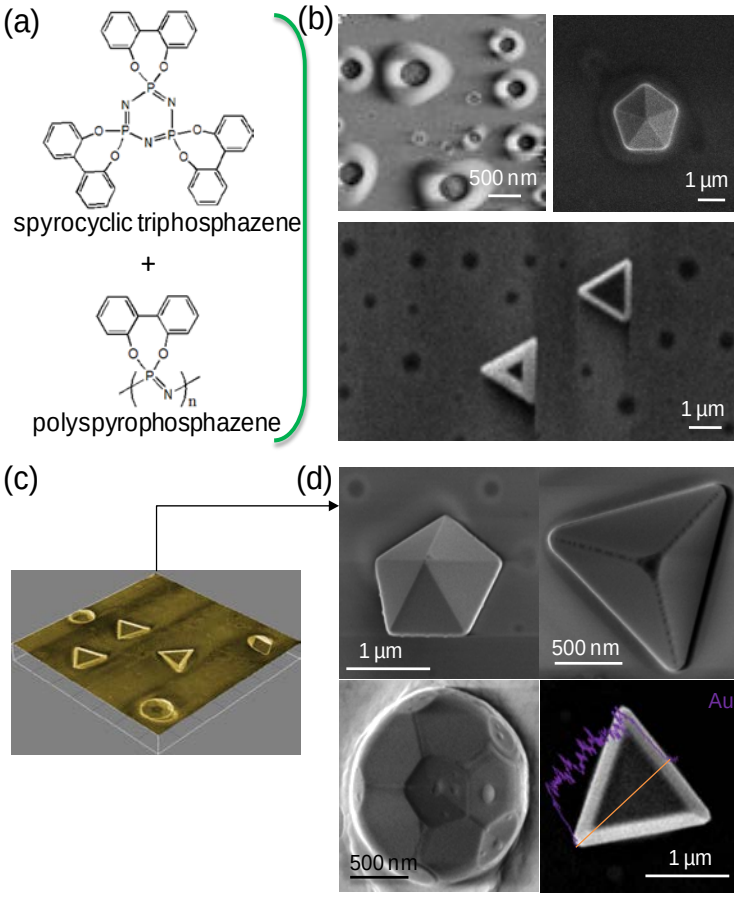


Figure 7. (a) Structure of mixtures using in conjunction with Au-containing organometallics. (b) AFM and SEM analysis of surface pinholes features formed during microphase demixing of the mixture and subsequent coarsening and ripening of Au NPs for form individual crystals. (c, d) A range of exotic polyhedral single crystal gold crystals such as a decahedron, tetrahedron, truncated icosahedra (fullerene) and EDX line mapping analysis confirming single phase gold composition.

As recently discussed anisotropy in micro and nanocrystals can led to an unprecedented diversity in new exotic crystalline shapes with interesting and unexpected properties [45, 46]. These findings outline the possibility of controlling morphology, shape and size of gold crystals obtained by solid state reactions.

The marriage of polymer dewetting, demixing and spinodal decomposition to metal-coordinated macromolecular polymers augers well for a variety of important applications. Further insight into this issue would be gained by understanding the influence of the mixing parameters and structure of the precursors so controlled microphase demixing and dewetting processes, which are largely used in the understanding of thin liquid polymer film. Methods to stabilize unwanted dewetting, would allow bespoke metallic crystals in a fully solid state process and also have the potential for surface patterning inbuilt into the technique. Optimization of thickness and molecular weight will eventually allow more controlled instability formation in the polymer, which will lend itself to metal crystals and structures not possible through solution based routes.

## SILVER, PALLADIUM AND RHENIUM CRYSTAL GROWTH: SOLID STATE PYROLYSIS OF AGPPH3[CF3SO3] /[NP(O2C12H8)]N AND PDCL2/[NP(O2C12H8)]N MIXTURES

Similar to the Au-phosphazene mixtures, the pyrolysis of $AgPPh_3[CF_3SO_3]/[NP(O_2C_{12}H_8)]_3$ and $PdCl_2/[NP(O_2C_{12}H_8)_3$ mixtures at 800 °C under air can result in Ag and Pd nanoparticles and microcrystals identified mainly by powder XRD and HRTEM with electron diffraction. Specifically, the mechanism of the macromolecular precursor deposition under heating is similar, with cleavage of metal centers and their subsequent agglomeration to single crystal nanoparticles. Demixing of the metal- and non-metal-containing phases within the mixture allows spatial patterning due to nucleation dewetting processes. In all cases for all metals thus far studied, carbonization and graphitization of the resulting carbon residue prevent full dewetting of the layer which gives a high density of crystals on the surface. Figure 8 summarizes the stages of decomposition, nanoparticles formation and resulting high surface area porous Ag and Pd foams formed from each precursor at high metal loading.

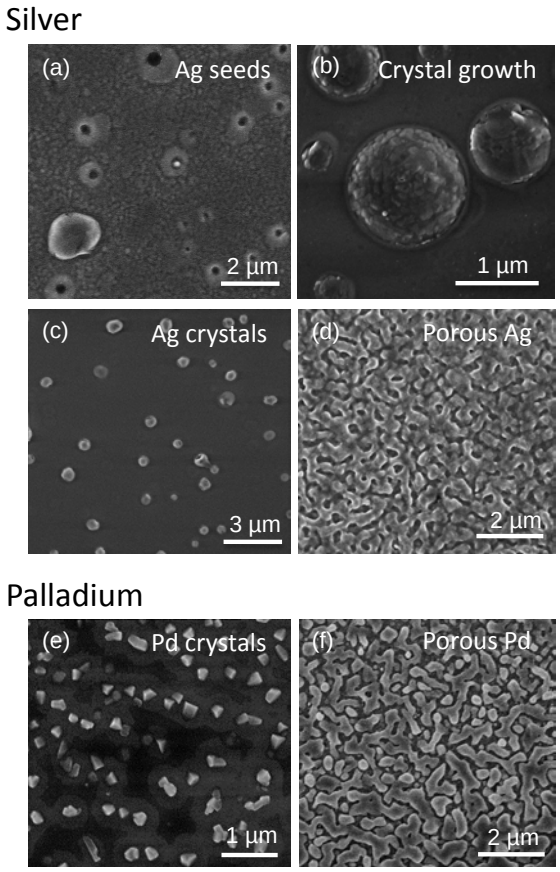


Figure 8. Evidence for a similar mechanism successfully applied to Ag and Pd. (a) NP and seed formation within pinhole voids (b) growth of the metal within the pinhole voids (c) faceted crystals that grow from pinholes (d) and porous metal foams. (e) nucleation dewetting formation of sub-micron Pd crystals and (f) corresponding porous Pd.

It is interesting to note that although several solution-based methods also exist for prepare Pd nanoparticles have been reported [47-57], relatively few solid state routes are known [57]. Usefully, thermolysis of $[Pd(S_{12}C_{12}H_{22})_2]_6$ gives Pd nanoparticles but mixed with PdO and PdS [58]. Using our method, both microcrystals and nanoparticles can be formed in addition to porous foams, depending on the concentration of Pd, which affects not only the chemical decomposition but also the demixing of the two polymeric-type phases during heating; low concentration results in NPs, high concentration results in porous metals.

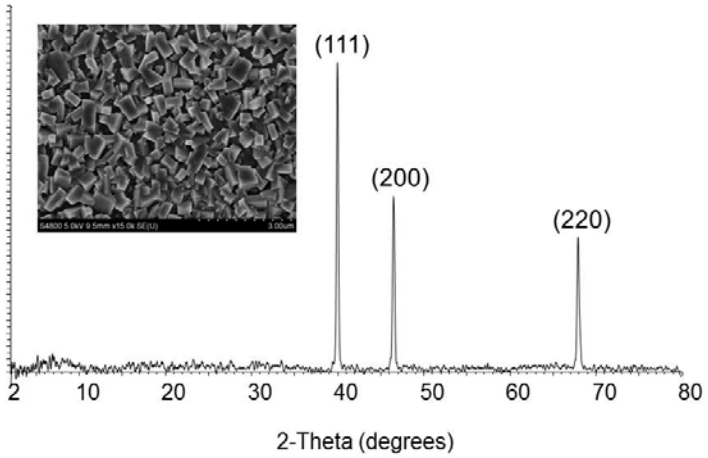


Figure 9. X-ray diffraction pattern for $PdCl_2/N_3P_3[O_2C_{12}H_8]_3$ precursor after pyrolysis confirming single crystal Pd. The inset is a SEM image of the cubic-like Pd microcrystals formed.

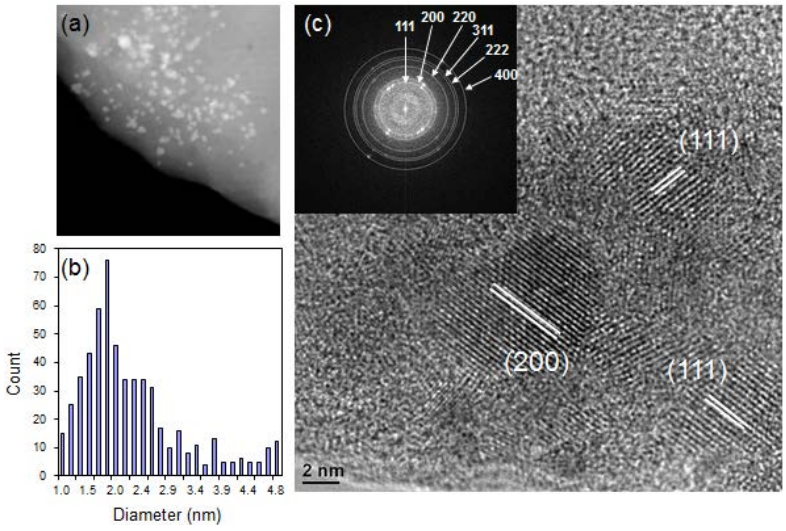


Figure 10. HAAD STEM image of Pd nanoparticles formed within the demixed polymer matrix. (b) Size distribution analysis of Pd particles confirming a log-normal distribution consistent with Ostwald ripening of the NPs. (c) HRTEM image of individual Pd NPs. (d) The inset shows the corresponding selected area electron diffraction pattern confirming the cubic Fm3m space group.

SEM and XRD show in in Figure 9 confirms this. Additionally, HRTEM analysis of the Pd nanoparticle and microcrystals confirms that they form as

single crystals, much like the situation for Au and Ag, and be a similar overall chemical and physical decomposition mechanisms, and without unwanted oxide and sulfide phase formation. Figure 10 shows the variation in nanoparticle diameters for Pd synthesized using the SSPM method. With low Pd content and high mixture or C content, small nanoparticles with diameters as small as ~2.5 nm (averaged from ~800 NPs) are found with a log-normal size distribution.

## THE CASE OF RHENIUM CRYSTAL GROWTH: PYROLYSIS OF K[REO4]/[NP(O2C12H8)]3

The practical importance of Rhenium arises from its multiple uses as an element of superalloys typically employed in rotating elements of aircraft engines, as barrier layers and can be used in the enhancement of interfacial properties of microelectronic conductors.

Additionally, Re compounds have useful catalytic activity in several hydrocarbon transformations and selective reduction of $NO_x$. It also has catalytic applications for hydrodesulfurization, hydrodenitrogenation and highly selective oxidation of methanol. However few reports on nanostructured Re have appeared [59-68].

In a review by Méndez [59], only two reports on Re films [60, 61] are mentioned and were limited to spectroscopic identification. This comprises the first report that claims the formation of nanostructured Re. Later, Hassel and coworkers reported the preparation of Re nanowires from a selected dissolution of a Ni/Al/Re alloy [62].

However, the characterization was performed only by SEM and EDAX techniques. Subsequently Philippe [63] studied the hardness properties of Re nanowires prepared by this latter method. From deposition of films of $NH_4ReO_4$, films of Re were identified by SEM and XPS [64]. Nanoparticles of 3 nm in size have also been observed by TEM and characterized by powder XRD. More recently, nanoparticles of Re were prepared from $ReCl(CO)_3(N,N)$ [65] and $Re_2(CO)_{10}$ [66] using ionic liquids as stabilizing agents. Some catalytic applications on ammonia synthesis [67-68] and glycerol conversion have been reported [68] have been reported.

Using the SSPM method, pyrolysis of the $K[ReO_4]/[NP(O_2C_{12}H_8)]_3$ mixtures satisfyingly produced pure Re as single crystal microcrystals and nanoparticles.

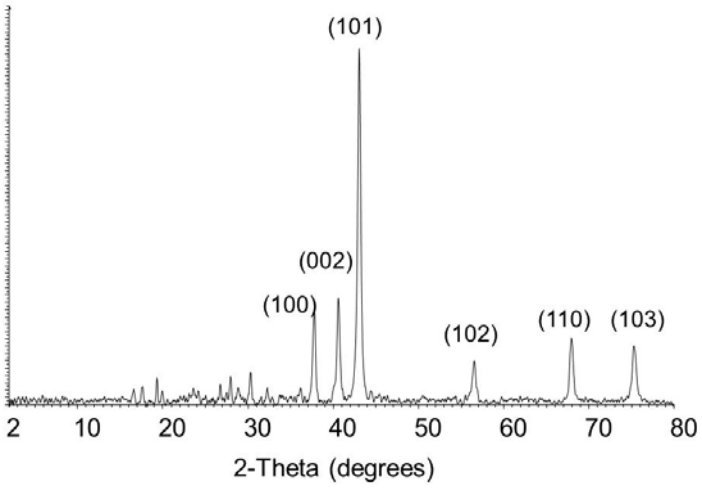


Figure 11. X-ray diffraction pattern from the pyrolytic product from 1:5 $K[ReO_4]$ /$[NP(O_2C_{12}H_8)]_3$ mixture.

Again, incubation of NPs that coarsen to pinholes formed within the carbon residue allow the ripening growth of individual structure on surfaces, thus forming the first successfully solid state approach to size control individual single crystals of Re. X-ray as indicated by the XRD pattern see Figure 11. The planes corresponding to (100), (002), (101), (102), (110), and (103) reflections from hexagonal Re are clearly observed.

Figures 12a and b show that Re microcrystals with quasi-spherical morphologies and rough, layered outer surfaces similar to a nautilus structure formed by growth from within a carbon pinhole on the surface. Each particle grows from within each of these pinholes. For a given Re quantity and mixture ratio, the shape and yield of the Re particles can be varied. For instance, in Figure 12c using half the quantity of Re with respect to the overall *i.e.* a 1:5 mixture ratio of $K[ReO_4]/[NP(O_2C_{12}H_8)]_3$, deposited on $SiO_2$, faceted polyhedral microcrystals are found, as opposed to circular crystals. In Figure 12a, the spherical microcrystals are found to grow from pinhole voids following the typical route for this solid state method. For lower Re quantities, such as with the 1:10 $K[ReO_4]/[NP(O_2C_{12}H_8)]_3$ mixture for example, the resulting crystals are nucleated on the surface as shown in Figure 12b, and subsequent growth allow the definition of polyhedral crystals of Re.

Additionally, the size control extends down to the nanoscale where high quality nanoparticles and nanocrystals of pure Re are possible by this method. Dark-field scanning TEM was used to highlight high atomic number materials

such as noble metals by their propensity for high angle electron scattering, and also to avoid carbon degradation or in-situ formation of particles under the beam. Dark field STEM shown in Figure 13a indicates nanoparticle formation with a range of sizes from pyrolysis of a 1:5 $K[ReO_4]/[NP(O_2C_{12}H_8)]_3$ precursor mixture. Analysis of >700 particles confirms that the mean diameter is 2.9 nm (when the larger particles >15 nm are ignored), see Figure 13d. HRTEM EDX shown in Figure 13b also confirms the identification of pure Re.

The nanoparticles were all confirmed to be single crystal. Typically, when growing metallic nanoparticles from solution, thermodynamically unfavoured shapes are very common and control over the subsequent growth depends on the liquid-borne seed being single crystal. All NPs formed with the metals reported here are single-crystal, and Re is no different. The lattice resolution HRTEM image in Figure 13c and corresponding FFT pattern are indexed to Re in the hexagonal unit cell with space group $P6_3/mmc$ and cell parameters a = 0.276 nm and c = 0.445 nm.

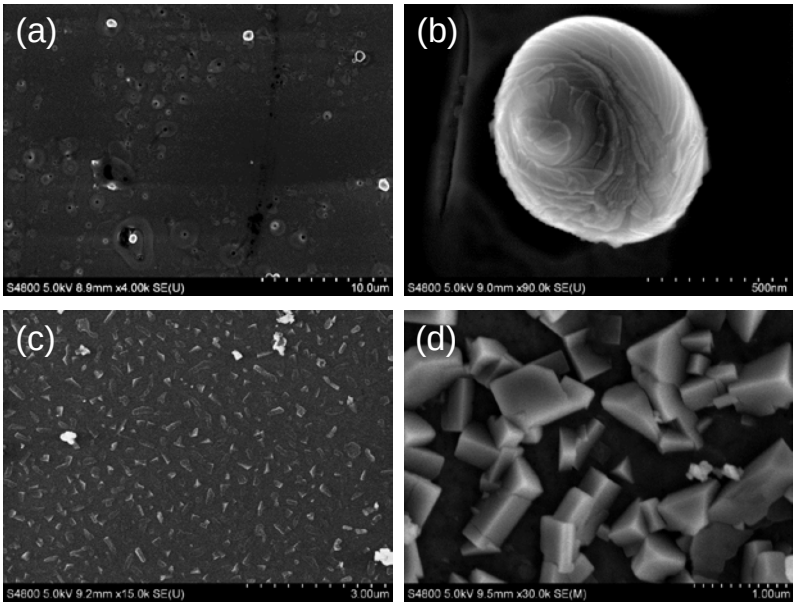


Figure 12. SEM images of Re crystal growth on surfaces using the SSPM method for 1:5 $K[ReO_4]/[NP(O_2C_{12}H_8)]_3$ precursor mixtures. Single crystal Re is formed (a,b) quasi-spherical micron sized particles from pinhole voids in the demixed and decomposed polymeric mixture. (c,d) polyhedral Re crystals formed after pyrolysis of the mixture with half the quantity (1:10 ratio) of Re.

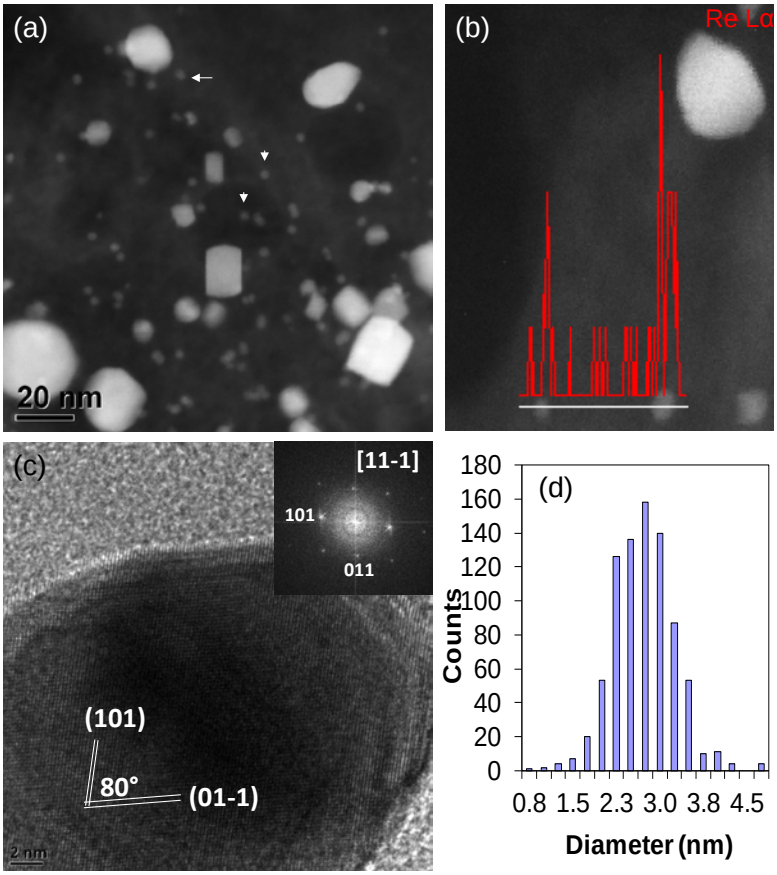


Figure 13. (a) Dark field STEM image of a range of nanoparticles of Re. (b) Nanoscale EDX of the Re L confirming that crystals are composed of Re. (c) Lattice resolution HRTEM image of a single Re nanoparticle confirming single crystal nature and (d) size distribution of ~700 nanoparticles from TEM measurements.

## INSIGHTS INTO THE FORMATION MECHANISM

Although the formation mechanism of Au nanoparticles has been widely studied and recently revised [69-73], the solid state mechanism for the formation of Au nanoparticles in solid state [35-40] has not been significantly investigated or clarified [5]. The most probable mechanism of formation of Au nanostructures involve the energetically easy loss of Cl to give a $PPh_3Au^+$ species which is known to interact the π system of the aryl groups of the

bispyro both of the polymer as well as the trimer [74-77]. These in turn afford a stable solid matrix which is not lost, as a volatile, in the first stage of the annealing.

Subsequently oxidation of the organic matter gives rise to holes where the metallic gold begins to agglomerate, nucleate and grow. It is at this stage, the mixture contains single crystal NPs of gold. In parallel, thermal decomposition of the mixture in the form of phase separation also occurs, where the instability is driven by nucleation dewetting and the formation of pinhole voids within the solidifying mixture. The result in the growth of crystal from within these incubation sights by Ostwald ripening of the migrating Au nanoparticles.

The pinholes act as a nucleation point and are pinned to the surface and thus all nanoparticles for Au and Ag, for example, migrate towards these holes. This occurs for cases in which the metal content is sufficiently low; higher metal content results in a spinodal decomposition of the demixed polymer mixture to give porous metal foam structures. Further evidence for Au-content influence on nanoscale decomposition is found in Figure 14a, where for polymer mixture with little or no gold content, characteristic Voronoi tessellation patterns consistent with classical polymeric dewetting is found. The reason for the observation of unfinished tessellation or beading pattern is due to the solidification and carbonization of the organic matter, which eventual graphitizes.

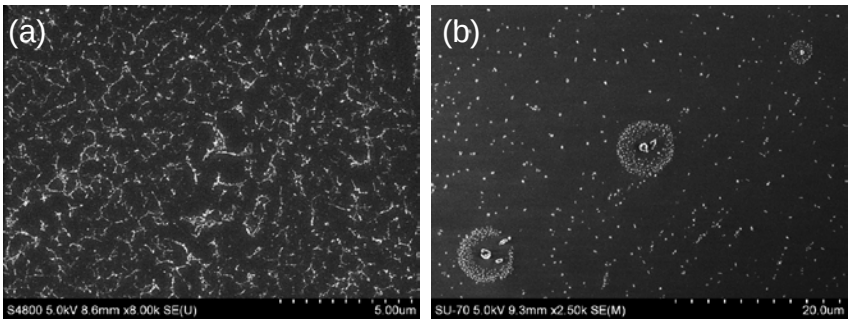


Figure 14. (a) Voronoi-like dewetting of a polymer film without metal content. Unlike liquid polymer films, complete tesselation pattern formation and dewetting cannot occur since a constant temperature ramp results in carbonization and solidification of the polymer. (b) SEM image of NP coalescence around a dust particle defect. This confirms a polymeric dewetting mechanism where in this case nucleation dewetting (up to the point of polymer solidification via carbonization and subsequent graphitization) causes NPs to characteristically form around the defects.

While specific decomposition chemistry occurs in all cases to result in the initial nanoparticles of Au, detailed below, the overall pattern is driven by physical dewetting and most of the characteristics are that of nucleation dewetting occurring during the demixing of two bicontinuous phases. Introducing surface defects has a specific influence on such systems, where dirt acts as a nucleation point for mobile surface-bound (NPs at the surface-air interface) and polymer-bound nanoparticles. Figure 14b shows this precisely, where nucleation of surface bound NPs surrounds surface defects and mimics the profile of the defect, confirming NP coarsening to surface pinned defects through a competition between particle and surface interaction potential mediated by the viscosity, mobility, mixture thickness that ultimately tune the Hamaker constants between each material. If the defect is a pinhole formed during demixing, as seen in Figures 7 and 8, then the NPs aggregated and ripen to form single crystals of the respective metal coordinated to the organometallic fragment.

At the molecular level, the case of the $N_3P_3(O_2C_{12}H_8)_3$/$AuCl(PPh_3)$ and $[NP(O_2C_{12}H_8)]_n$/$AuCl(PPh_3)$ mixtures shows that a strong Au-arene interaction between the $Au(PPh_3)^+$ cationic centers and biphenyl rings could permit a regular ordering of the Au centers along with the $NP(O_2C_{12}H_8)$ groups of the chains of the polymer or around the cyclic molecules of the trimer, as depicted in Figure 7b. Figure 15 summarizes a plausible general structure of the molecular level decomposition and cyclomatrix formation and the nanoscale demixing of phases, for the case of Au. Au(I)-arene interactions have been recently discussed by Laguna *et al.* [74-77]. Intermolecular gold-arenes have been reported in the trinuclear complex $Au_3$(p-tolN=COEt)$_3$ [75]. Also metal-arene interactions have been observed in the one dimensional array supramolecular structures of the gold(I) complex [Au(CN){2,6-$NC_5H_3(C_6H_4)_2$-C,C'N}] [76]. Intramolecular metal-arene interactions have been also observed in some complexes. Recently strong M-arene interactions (M = Au, Ag, Cu) have been reported in metal-dialkylbiarylphosphane complexes [78]. It is likely that a similar mechanism operates for all metals reviewed here so as to form the nanoparticles which influence the ultimate demixing and dewetting of the polymer film.

The results presented here show that the formation of metallic nanostructures does not require the covalent linking of the organometallic fragment to the polymeric or trimeric phosphazenes structures. Thus the size of the Au nanoparticles can be controlled by selecting the appropriate mixture for the precursor, *e.g.* $[NP(O_2C_{12}H_8)]_n$/$AuCl(PPh_3)$ or $[NP(O_2C_{12}H_8)_3]$/ $AuCl(PPh_3)$ and an adequate preparation procedure.

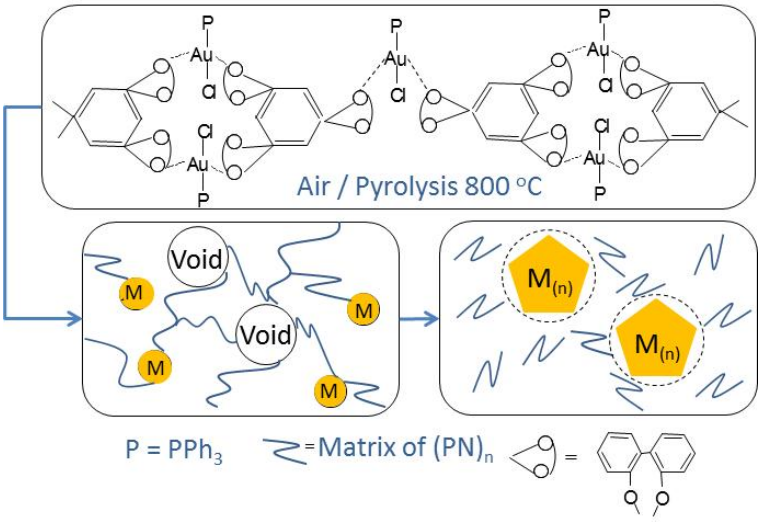


Figure 15. Proposed mechanism of the pyrolysis of a $N_3P_3(O_2C_{12}H_8)_3$/AuCl($PPh_3$) mixture as a precursor to metallic crystal formation in the solid state.

It is interesting to note that using this method, Au nanoparticles as small as 3.5 nm can be obtained, with a mean size of ~5 nm. As is known for gold, at ultrasmall NP sizes (typically <2 nm) quantum size effects start to be manifested. The main advantage of the preparation of solid Au nanoparticles is that the nanoparticles do not requires stabilizing molecules. In this method the presence of the $N_3P_3(O_2C_{12}H_8)_3$ or $N_3P_3(O_2C_{12}H_8)_n$ is crucial because solid state pyrolysis of AuCl($PPh_3$) results in bulk Au agglomerates.

Phase separation is expected in asymmetric polymer-particle mixtures [78-80] for large particle-to-monomer size ratios. As in polymer mixtures, increasing the molecular mass should increase the critical point [81] and result in phase separation. Further, an entropically driven surface phase transition has been observed [82], and predicted [34,84] for low-Mw polymer-particle thin films, resulting in the expulsion and layering of NPs along the solid substrate. Early stages of spinodal decomposition are generally described by Cahn-Hilliard theory [85] yielding a dominant wavelength, which then grows via a number of coarsening mechanisms [86].

We rationalize these observations in terms of the entropic-driven phase separation of $[NP(O_2C_{12}H_8)]_n$/AuCl($PPh_3$) or $[NP(O_2C_{12}H_8)_3]$/AuCl($PPh_3$) mixtures, followed by Au association, observed in the bulk above a threshold temperature [87] into a ripening phase that is surface pinned, enveloped by a $[NP(O_2C_{12}H_8)]_n$ or $[NP(O_2C_{12}H_8)_3]$ rich phase that converts to carbon during

pyrolysis, much like in thin film polymer mixtures with asymmetric surface attraction [88,89]. We interpret this behavior as an interplay between polymer-particle miscibility and particle-surface attraction via entropic pushing, occurring in a polymer matrix with known viscosity and film thickness. Low-Mw thin composite films have been shown to form a diffuse layer of NPs at the substrate interface after spin coating which failed to be redispersed by subsequent thermal annealing. The formation of micron-sized irregular NP clusters at the substrate interface, instead of a uniform surface monolayer, has also been recently reported on relatively thick spun-cast films of PS(600k) with 5% $C_{60}$ [90]. In the SSMP method, the situation is markedly improved where this bicontinuous phase separation is driven by dewetting where NPs form due to the chemical decomposition and crystals eventually grow due to the physical decomposition. While all other know systems separate to form aggregates, this method allows single crystal growth via ripening, rather than simply disordered coalescence. Nanoparticle diffusion in thin films is strongly anisotropic (considerably faster in the plane of the film direction) and the viscosity of high-Mw composite films correspondingly higher, tuning the interplay between surface attraction and phase separation.

## CONCLUSIONS

Metallic foams and nanoparticles can now be easily prepared from mixtures of polymeric or cyclic phosphazenes and organometallic complexes containing noble metals. For Au, it has been shown that the variation of the phosphazene/Au ratios allows for the formation of either metallic foams of high density or discrete Au polyhedral crystals and also nanoparticles, whose mean size and morphology are controlled through the structure of the precursor constituents and the relative ratio in the mixtures. With the $[NP(O_2C_{12}H_8)]_n$/$AuCl(PPh_3)$ mixtures, Au nanoparticles of 3.5 nm diameter are obtained from films formed by pyrolysis of the 1:1 mixture ratio, while with the analogous 1:1 mixture of $N_3P_3(O_2C_{12}H_8)_3$/$AuCl(PPh_3)$ resulted in Au nanoparticles with a mean diameter of 4.7 nm from a powder deposit. For a given Re quantity and mixture ratio, the shape and yield of the Re particles can be varied. Using a 1:5 mixture ratio of $K[ReO_4]$/$[NP(O_2C_{12}H_8)]_3$, deposited on $SiO_2$, faceted polyhedral microcrystals are found, as opposed to circular crystals. For lower Re quantities, such as with the 1:10 $K[ReO_4]$/$[NP(O_2C_{12}H_8)]_3$ mixture, the resulting crystals are nucleated on the surface, and subsequent growth allow the definition of polyhedral crystals of

Re. Nanoparticle formation with a range of sizes was possible from pyrolysis of a 1:5 $K[ReO_4]/[NP(O_2C_{12}H_8)]_3$ precursor mixture. Analysis of >700 particles confirms that the mean diameter is 2.9 nm. Extension to Ag and Pd also resulted in micro and nanoparticle crystals using similar polymeric precursors, including high surface area porous Ag and Pd, nanoparticles and microcrystals. Additionally, a comparison with previous studies shows that the formation of metallic nanostructures does not require the covalent linking of the organometallic fragment to the polymeric or trimeric phosphazenes, although the presence of the cyclic or polymeric phosphazene as solid state template is necessary to incubate seeds and crystal growth.

This method for preparing Au, Ag, Pd, and Re noble metal nanostructured materials completely in the solid state is potentially useful in the fabrication of solid-sate device contacts and interconnects in the field of electronics, as nanoparticle embedded materials for chemical sensing/detectors and catalysis, and also as surface plasmon-mediated sensors or support materials. Controlling surface bound NP concentrations and position through dewetting allow the possibility for single-step SERS substrates exploiting plasmon 'hot-spots' from NP pairs or clusters in close proximity. Importantly, the method allows the deposition of metallic materials in the complete absence of water or liquids. Phase demixing also has potential for precursor tuning (Mw, viscosity, dielectric constant, metal concentration etc.) for patterning purposes similar to block-copolymer patterning via phase separation or demixing, with the added ability to form perfect polyhedral crystals in the solid state in parallel.

## ACKNOWLEDGEMENTS

The authors thank Fondecyt (project 1085011) for financial support. We also thank to Professor G.A. Carriedo from the University of Oviedo, Spain, for valuable collaboration in the work cited in this chapter.

## REFERENCES

[1] C. N. R. Rao, A. Muller, A. K. Cheetham, (Eds). *The Chemistry of Nanomaterials*, Wiley-VCH, Weinheim, Germany (2004).

[2] S. Edelstein, R. C. Cammarata, (Eds). *Nanomaterials: Synthesis, Properties and Applications*, J.W. Arrowsmith Ltd, Bristol, UK (1998).

[3] K. J. Klabunde, (Ed). *Nanoscale Materials in Chemistry*, Wiley and Sons, New York (2001).
[4] C. Díaz, M. L. Valenzuela, Chapter 16, *Encyclopedia of Nanoscience and Nanotechnology*, H. S. Nalwa, (Ed). American Scientific Publishers (2011).
[5] P. E. Chow, Chapter 14, *Gold Nanoparticles: Properties, Characterization and Fabrication*, Nova Science Publishers (2010).
[6] G. B. Khmutov V. V. Kislov, M. N. Antipirina, R. V. Gainutdinov, S. P. Gubin, A. N. Sergeev-Cherenkov, E. S. Soldatov, D. B. Suyatin, A. L. Tolstikhina, A. S. Trifonov and T. V. Yurova, *Microelectron. Eng.* 69, 373 (2003).
[7] E. C. Walters, K. Ng, M. P. Zach, R. M. Penner and F. Favier, *Microelecton. Eng.* 61, 62 (2002).
[8] G. Walters and I. Parkin, *J. Mater. Chem.* 19, 574 (2009).
[9] C. Díaz and M. L. Valenzuela, *J. Chil. Chem. Soc.* 50, 417 (2005).
[10] C. Díaz, P. Castillo and M. L. Valenzuela, *J. Cluster Sci.* 16, 515 (2005).
[11] C. Díaz and M. L. Valenzuela, *J. Inorg. Organomet. Polym. Mater.* 16, 123 (2006).
[12] C. Díaz and M. L. Valenzuela, *Macromolecules* 39, 103 (2006).
[13] C. Díaz and M. L. Valenzuela, *J. Inorg. Organomet. Polym. Mater.* 16, 216 (2006).
[14] C. Díaz and M. L. Valenzuela, *J. Inorg. Organomet. Polym. Mater.* 6, 419 (2006).
[15] C. Díaz, M. L. Valenzuela, L. Zuñiga, C. O'Dwyer, *J. Inorg. Organometallic Polymer*, 19, 507 (2009).
[16] C. Diaz, M. L. Valenzuela, D. Bravo, V. Lavayen and C. O'Dwyer, *Inorg. Chem.* 47, 11561 (2008).
[17] C. Díaz, M. L. Valenzuela, E. Spodine, Y. Moreno and O.Peña, *J. Clust. Sci.* 18, 831 (2007).
[18] C. Díaz, M. L. Valenzuela and S. Ushak, *J. Clust. Sci.* 19, 471 (2008).
[19] J. Jimenez, A. Laguna, M. Benouazzane, J. A. Sanz, C. Díaz, M. L. Valenzuela, P. G. Jones, *Chem. Eur. J.* 15, 13509 (2009).
[20] C. Diaz, M. L. Valenzuela, A. Laguna, V. Lavayen, J. Jimenez, L. Power and C. O'Dwyer, *Langmuir* 26, 10223 (2010).
[21] C. Diaz, V. Lavayen, and C. O'Dwyer, *J. Solid State Chem.* 183, 1595 (2010).
[22] G. A. Carriedo, M. L. Valenzuela, C. Diaz and S. Ushak, *Eur. Polym. J.* 44, 686 (2008).

[23] C. Díaz, M. L. Valenzuela, S. Ushak, V. Lavayen and C. O'Dwyer, *J. Nanosci. Nanotechnol.* 9, 1825 (2009).
[24] C. Díaz, M. L. Valenzuela and N. Yutronic, *J. Inorg. Organomet. Polym. Mater.* 17, 577 (2007).
[25] C. Díaz, M. L. Valenzuela, G. A. Carriedo, F. J. Garcia Alonso, A. Presa, *Polym. Bull.* 57, 913 (2006).
[26] C. Diaz, M. L. Valenzuela, G. A. Carriedo, L. Zuñiga and C. O'Dwyer, *J. Inorg. Organomet. Polym. Mater.* In press doi:10.1007/s10904-011-9601-8
[27] M. Hodge, J. R. Hayes, J. A. Caro, J. Biener, A. Nhamza, *Adv. Eng. Mater.* 8, 853 (2006).
[28] C. Tappan, M. H. Huyuh, M. A. Hiskey, D. E. Chavez, E. P. Luther, I. T. Mang, S. F. Son, *J. Am. Chem. Soc.* 128, 6589 (2006).
[29] Banhart, *Adv. Eng. Mater.* 8, 781 (2006).
[30] H. Ehang, A. I. Cooper, *J. Mater. Chem.* 15, 2157 (2005).
[31] Biener, G. W. Nyce, A. M. Hodge, M. M. Biener, A. V. Hamza, S. A. Maier, *Adv. Mater.* 20, 211 (2008).
[32] Y. Ding, J. Enlabacher, *J. Am. Chem. Soc*. 125, 772 (2003).
[33] F. Khan, S. Mann, *J. Phys. Chem. C* 113, 19871 (2009).
[34] T. Teranishi, S. Hasegawa, T. Shimizu, M. Miyake, *Adv. Mater.* 13, 1699 (2001).
[35] T. Shimizu, T. Teranishi, S. Hasegawa, M. Miyake, *J. Phys. Chem. B.* 107, 2719 (2003).
[36] M. Miyake, W. Zheng, F. L. Leibowitz, N. K. Ly, Ch. Zhong, *Langmuir* 16, 490 (2000).
[37] Oiu, X. Jiang, C. Zhu, M. Shirai, J. Si, N. Jiang, K. Hirao, *Angew. Chem. Int. Ed*. 43, 2230 (2004).
[38] G. Lusvardi, G. Malavasi, V. Aina , L. Bertinetti, G. Cerrato, G. Magnacca, C. Monterra and L. Menabue, *Langmuir* 26, 10303 (2010).
[39] Eichelbaum, K. Rademann, R. Muller, M. Radtke, H. Riesemeier, W. Gorner *Angew. Chem. Int. Ed.* 44, 7905 (2005).
[40] G. A. Carriedo, L. Fernández-Catuxo, F. J. García Alonso, P. Gómez-Elipe, P. A. González, *Macromolecules* 29, 5320 (1996).
[41] Sánchez-Iglesias, I. Pastoriza-Santos, J. Pérez-Juste, B. Rodríguez-González, F. J. García de Abajo and L. M. Liz-Marzán, *Adv. Mater.* 18, 2529 (2006).
[42] R. Levi, M. Bar-Sadan, A. Albu-Yaron, R. Popovitz-Biro, L. Houben, Ch. Shahar, A. Enyashin, G. Seifert, Y. Prior, R. Tenne, *J. Am. Chem. Soc.* 132, 11214 (2010).

[43] R. Tenne, G. Seifert, *Ann. Rev. Mater. Res*. 39, 387 (2009).
[44] R. Tenne, *Chem. Eur. J*. 8, 5297 (2002).
[45] S. C. Glotzer, M. J. Solomon, *Nat. Mater*. 6, 557 (2007).
[46] Halder, P. Kundu, B. Viswanath, N. Ravinshankar, *J. Mater. Chem.* 20, 4763 (2010).
[47] J. Turkevich, G. Kim, *Science* 169, 873 (1970).
[48] J.G. de Vries, *J.C.S. Dalton Trans* 421 (2006).
[49] T. Teranishi and M. Miyake, *Chem. Mater*. 10, 594 (1998).
[50] P. John Thomas, G. U. Kulkardin, and C. N. R. Rao, *J. Phys. Chem*. 104, 8138 (2000).
[51] Y. Sun, L. Zhang, H. Zhou, Y. Zhu, E. Sutter, Y. Ji, M. H Rofailovich, J.C Sokolov, *Chem. Mater.* 19, 2065 (2007).
[52] M. T. Reetz, W. Heilbirg, *J. Am. Chem. Soc*. 116, 7401 (1994).
[53] E. Ramirez, S. Jonsat, K. Philippol, P. Lecante, M. Gomez, A. M Masden Bulto, B. Chaudret*; J. Organomet. Chem*. 589, 4601 (2004).
[54] N. Anil Dhor and A Godenken, *Chem. Mater.* 8, 445 (1998).
[55] G. Cardenas Trivino, K. J. Klabunde and E. Broca Dale, *Langmuir* 3, 986 (1987).
[56] Y. Yu, Y. Zhao, T. Huang and H. Liu, *Pure Appl. Chem.* 81, 2377 (2009).
[57] H. Chen, G.Wei, A. Ispas, S. G. Hickey and A. Eychmuller, *J. Phys. Chem*. C 114, 21976 (2010).
[58] D. Jose, B. R Jagida, *J. Solid State Chem.* 183, 2059 (2010).
[59] E. Mendez, M. F. Cerdà, A. M. Castro Luna, C. F. Zinola, C. Kremer, M. E. Martins, *J. Colloid Interface Sci.* 263, 119 (2003).
[60] R. Schrebler, P. Cury, M. Orellana, H. Gòmez, R. Còrdova, E.A. Dalchiele, *Electrochim. Acta* 46, 4309 (2001).
[61] J. Zerbino, A. M. Castro Luna, C. F. Zinola, M. E. Martins, *React. Kinet. Chem.* 521, 763 (2002).
[62] W. Hassel, B. Bello, Rodriguez, S. Milenkovic, A. Schneider, *Electrochim. Acta* 51, 795 (2005).
[63] L. Philippe, Z. Wang, I. Peyrot, A.W. Hassel, J. Michler, *Acta Materialia* 57, 4032 (2009).
[64] O. A. Nikonova, K. Jansson, V. G. Kessier, M. Sundberg, A. I. Baranov, A. V. Shevelkov, D. V. Drobot, G. A. Seisenbaeva, *Inorg. Chem.* 47, 1295 (2008).
[65] R. R. Dykeman, N. Yan, R. Scopelliti, P. J. Dyson, *Inorg. Chem.* 50, 717 (2011).

[66] Vollmer, E. Redel, K. Abu-Shandi, R. Thomann, H. Manyar, C. Hardacre, C. Janiak, *Chem. Eur. J.* 16, 3849 (2010).
[67] F. Hayashi, M. Iwamoto, *Micro. Meso. Mater.* (2011). DOI: 10.10161/j.micromeso.2011.03.035.
[68] E. L. Kunkes, D. A. Simonetti, J. A. Dumesic, W. D. Pyrz, L. E. Murillo, J. G. Chen, D. J. Buttrey, *J. Catalysis* 260, 164 (2008).
[69] J. E. Millstone, S. J. Hurst, G. S. Metraux, J. I. Cutler, Ch. A. Mirkin, *Small* 5, 646 (2005).
[70] L. Malfatti, D. Morongiu, S. Costacurta, P. Falcaro, H. Amenitsch, B. Marmiro, J. Li, G. Crenci, M. F. Casula, P. Innocenzi, *Chem. Mater.* 22, 2132 (2010).
[71] J. Polte, T. T. Ahner, F. Delissen, S. Sokolov, F. Emmerling, A. F. Thunemann, R. Kraehnert, *J. Am. Chem.Soc*. 132, 129 (2010).
[72] X. Ji, X. Song, J. Li, Y. Bai, W. Yang, X. Peng, J. Am.Chem.Soc. 129, 13939-13948 (2007).
[73] K. Pong, H. I. Elim, J. X. Chong, W. Ji, B. L. Trout, J. Y. Lee *J.Phys.Chem. C* 111, 628 (2007).
[74] Laguna, *Modern Supramolecular Gold Chemistry*, Chapter 5, p. 318, Wiley-VCH, Wenheim (2008).
[75] R. A. Rawashdeh-Omary, M. A. Omary, J. P. Fackler, R. Galassi, B. R. Pietroni, A. Burini, *J. Am. Chem. Soc*. 123, 9689 (2001).
[76] A. Mohamed, R. A. Rawashdeh-Omary, M. A. Omary, J. P. Fackler, *Dalton Trans.* 2597 (2005).
[77] P. Perez-Galan, N. Delpont, H. Guerrero-Gomez, F. Maseras, A. M. Echavarren, *Chem. Eur. J*. 16, 5324 (2010).
[78] P. Paricaud, S. Varga, and G. Jackson, *J. Chem. Phys*. 118, 8525 (2003).
[79] G. J. Fleer and R. Tuinier, *Adv. Colloid Interface Sci.* 143, 1 (2008).
[80] J. B. Hooper, K. S. Schweizer, T.G. Desai, R. Koshy, and P. Keblinski, *J. Chem. Phys.* 121, 6986 (2004).
[81] J. Dudowicz, J. F. Douglas, and K. F. Freed, *J. Phys. Chem. B* 113, 3920 (2009).
[82] M. E. Mackay, Y. Hong and M. Jeong, S. Hong and T. P. Russell, C. J. Hawker, R. Vestberg, J. F. Douglas, *Langmuir* 18, 1877 (2002).
[83] S. McGarrity, A. L. Frischknecht, L. J. D. Frink, and M. E. Mackay, *Phys. Rev. Lett*. 99, 238302 (2007).
[84] S. McGarrity, A. L. Frischknecht, and M. E. Mackay, *J. Chem. Phys*. 128, 154904 (2008).
[85] J. W. Cahn and J. E. Hilliard, *J. Chem. Phys.* 31, 688 (1959).

[86] J. D. Gunton, M. San-Miguel, and P. S. Sahni, *Phase Transitions and Critical Phenomena*, Vol. 8, p. 267, C. Domb and J. L. Lebowitz (Eds). Academic, New York (1983).
[87] H. C. Wong, A. Sanz, J. F. Douglas, and J. T. Cabral, *J. Mol. Liq*. 153, 79 (2010).
[88] L. Sung, A. Karim, J. F. Douglas, and C. C. Han, *Phys. Rev. Lett.* 76, 4368 (1996).
[89] B.D. Ermi, A. Karim, and J. F. Douglas, *J. Polym. Sci. B* 36, 191 (1998).
[90] J. T. Han, G.-W. Lee, S. Kim, H.-J. Lee, J. F. Douglas, and A. Karim, *Nanotechnology* 20, 105705 (2009).

S. E.